MINIMIZING FLOPS TO LEARN EFFICIENT SPARSE REPRESENTATIONS

Anonymous authors
Paper under double-blind review

ABSTRACT

Deep representation learning has become one of the most widely adopted approaches for visual search, recommendation, and identification. Retrieval of such representations from a large database is however computationally challenging. Approximate methods based on learning compact representations, have been widely explored for this problem, such as *locality sensitive hashing*, *product quantization*, and *PCA*. In this work, in contrast to learning compact representations, we propose to learn high dimensional and sparse representations that have similar representational capacity as dense embeddings while being more efficient due to sparse matrix multiplication operations which can be much faster than dense multiplication. Following the key insight that the number of operations decreases quadratically with the sparsity of embeddings provided the non-zero entries are distributed uniformly across dimensions, we propose a novel approach to learn such distributed sparse embeddings via the use of a carefully constructed regularization function that directly minimizes a continuous relaxation of the number of floating-point operations (FLOPs) incurred during retrieval. Our experiments show that our approach is competitive to the other baselines and yields a similar or better speed-vs-accuracy tradeoff on practical datasets.

1 INTRODUCTION

Learning semantic representations using deep neural networks (DNN) is now a fundamental facet of applications ranging from visual search (Jing et al., 2015; Hadi Kiapour et al., 2015), semantic text matching (Neculoiu et al., 2016), oneshot classification (Koch et al., 2015), clustering (Oh Song et al., 2017), and recommendation (Shankar et al., 2017). The high-dimensional dense embeddings generated from DNNs however pose a computational challenge for performing nearest neighbor search in large-scale problems with millions of instances. In particular, when the embedding dimension is high, evaluating the distance of any query to all the instances in a large database is expensive, so that efficient search without sacrificing accuracy is difficult. Representations generated using DNNs typically have a higher dimension compared to hand-crafted features such as SIFT (Lowe, 2004), and moreover are dense. The key caveat with dense features is that unlike bag-of-words features they cannot be efficiently searched through an inverted index, without approximations.

Since accurate search in high dimensions is prohibitively expensive in practice (Wang, 2011), one has to typically sacrifice accuracy for efficiency by resorting to approximate methods. Addressing the problem of efficient approximate *Nearest-Neighbor Search (NNS)* (Jegou et al., 2011) or *Maximum Inner-Product Search (MIPS)* (Shrivastava and Li, 2014) is thus an active area of research, which we review in brief in the related work section. Most approaches (Charikar, 2002; Jegou et al., 2011) aim to learn compact lower-dimensional representations that preserve distance information.

While there has been ample work on learning compact representations, learning sparse higher dimensional representations have been addressed only recently (Jeong and Song, 2018; Cao et al., 2018). As a seminal instance, Jeong and Song (2018) propose an end-to-end approach to learn sparse and high-dimensional hashes, showing significant speed-up in retrieval time on benchmark datasets compared to dense embeddings. This approach has also been motivated from a biological viewpoint (Li et al., 2018) by relating to a fruit fly's olfactory circuit, thus suggesting the possibility of hashing using higher dimensions instead of reducing the dimensionality.

In a similar vein, in this work, we propose to learn high dimensional embeddings that are sparse and hence efficient to retrieve using sparse matrix multiplication operations. In contrast to compact lower-dimensional ANN-esque representations that typically lead to decreased representational power, a key facet of our higher dimensional sparse embeddings is that they can have the same representational capacity as the initial dense embeddings. The core idea behind our approach is inspired by two key observations: (i) retrieval of d (high) dimensional sparse embeddings with fraction p of non-zero values on an average, can be sped up by a factor of $1/p$. (ii) The speed up can be further improved to a factor of $1/p^2$ by ensuring that the non-zero values are evenly distributed across all the dimensions. This indicates that sparsity alone is not sufficient to ensure maximal speedup; the distribution of the non-zero values plays a significant role as well. This motivates us to consider the effect of sparsity on the number of *floating point operations (FLOPs)* required for retrieval with an inverted index. We propose a penalty function on the embedding vectors that is a continuous relaxation of the exact number of FLOPs, and encourages an even distribution of the non-zeros across the dimensions.

We apply our approach to the large scale metric learning problem of learning embeddings for facial images. Our training loss consists of a *metric learning* (Weinberger and Saul, 2009) loss aimed at learning embeddings that mimic a desired metric, and a *FLOPs loss* to minimize the number of operations. We perform an empirical evaluation of our approach on the Megaface dataset (Kemelmacher-Shlizerman et al., 2016), and show that our proposed method successfully learns high-dimensional sparse embeddings that are orders-of-magnitude faster. We compare our approach to multiple baselines demonstrating an improved or similar speed-vs-accuracy trade-off.

The rest of the paper is organized as follows. In Section 3 we analyze the expected number of FLOPs, for which we derive an exact expression. In Section 4 we derive a continuous relaxation that can be used as a regularizer, and optimized using gradient descent. We also provide some analytical justifications for our relaxation. In Section 5 we then compare our method on a large metric learning task showing an improved speed-accuracy trade-off compared to the baselines.

2 Related Work

Learning Compact Representations, ANN. Exact retrieval of the top-k nearest neighbours is expensive in practice for high-dimensional dense embeddings learned from deep neural networks, with practitioners often resorting to *approximate nearest neighbours* (ANN) for efficient retrieval. Popular approaches for ANN include *Locality sensitive hashing* (LSH) (Gionis et al., 1999; Andoni et al., 2015; Raginsky and Lazebnik, 2009) relying on random projections, *Navigable small world graphs* (NSW) (Malkov et al., 2014) and hierarchical NSW (HNSW) (Malkov and Yashunin, 2018) based on constructing efficient search graphs by finding clusters in the data, *Product Quantization* (PQ) (Ge et al., 2013; Jegou et al., 2011) approaches which decompose the original space into a cartesian product of low-dimensional subspaces and quantize each of them separately, and *Spectral hashing* (Weiss et al., 2009) which involves an NP hard problem of computing an optimal binary hash, which is relaxed to continuous valued hashes, admitting a simple solution in terms of the spectrum of the similarity matrix. Overall, for compact representations and to speed up query times, most of these approaches use a variety of carefully chosen data structures, such as hashes (Neyshabur and Srebro, 2015; Wang et al., 2018), locality sensitive hashes (Andoni et al., 2015), inverted file structure (Jegou et al., 2011; Baranchuk et al., 2018), trees (Ram and Gray, 2012), clustering (Auvolat et al., 2015), quantization sketches (Jegou et al., 2011; Ning et al., 2016), as well as dimensionality reductions based on principal component analysis and t-SNE (Maaten and Hinton, 2008).

End to End ANN. Learning the ANN structure end-to-end is another thread of work that has gained popularity recently. Norouzi et al. (2012) propose to learn binary representations for the Hamming metric by minimizing a margin based triplet loss. Erin Liong et al. (2015) use the signed output of a deep neural network as hashes, while imposing independence and orthogonality conditions on the hash bits. Other end-to-end learning approaches for learning hashes include (Cao et al., 2016; Li et al., 2017). An advantage of end-to-end methods is that they learn hash codes that are optimally compatible to the feature representations.

Learning Sparse Representations. *Sparse deep hashing (SDH)* (Jeong and Song, 2018) is an end-to-end approach that involves starting with a pre-trained network and then performing alternate minimization consisting of two minimization steps, one for training the binary hashes and the other

for training the continuous dense embeddings. The first involves computing an optimal hash best compatible with the dense embedding using a *min-cost-max-flow* approach. The second step is a gradient descent step to learn a dense embedding by minimizing a metric learning loss. The idea of high dimensional sparse embeddings is also reinforced by the *sparse-lifting* approach (Li et al., 2018) where sparse high dimensional embeddings are learned from dense features. The idea is motivated by the biologically inspired *fly* algorithm (Dasgupta et al., 2017). Experimental results indicated that *sparse-lifting* is an improvement both in terms of precision and speed, when compared to traditional techniques like LSH that rely on dimensionality reduction.

ℓ_1 **regularization, Lasso.** The *Lasso* (Tibshirani, 1996) is the most popular approach to impose sparsity and has been used in a variety of applications including sparsifying and compressing neural networks (Liu et al., 2015; Wen et al., 2016). The *group lasso* (Meier et al., 2008) is an extension of lasso that encourages all features in a specified group to be selected together. Another extension, the *exclusive lasso* (Kong et al., 2014; Zhou et al., 2010), on the other hand, is designed to select a single feature in a group. Our proposed regularizer, originally motivated by idea of minimizing FLOPs closely resembles exclusive lasso. Our focus however is on sparsifying the produced embeddings rather than sparsifying the parameters.

Metric Learning. While there exist many settings for learning embeddings (Hinton and Salakhutdinov, 2006; Kingma and Welling, 2013; Kiela and Bottou, 2014) in this paper we restrict our attention to the context of metric learning (Weinberger and Saul, 2009). Some examples of metric learning losses include large margin softmax loss for CNNs (Liu et al., 2016), triplet loss (Schroff et al., 2015), and proxy based metric loss (Movshovitz-Attias et al., 2017).

3 Expected number of FLOPs

In this section we study the effect of sparsity on the expected number of FLOPs required for retrieval and derive an exact expression for the expected number of FLOPs. The main idea in this paper is based on the key insight that if each of the dimensions of the embedding are non-zero with a probability p (not necessarily independently), then it is possible to achieve a speedup up to an order of $1/p^2$ using an inverted index on the set of embeddings. Consider two embedding vectors $\boldsymbol{u}, \boldsymbol{v}$. Computing $\boldsymbol{u}^T\boldsymbol{v}$ requires computing only the pointwise product at the indices k where both $\boldsymbol{u}_k$ and $\boldsymbol{v}_k$ are non-zero. This is the main motivation behind using inverted indices and leads to the aforementioned speedup. Before we analyze it more formally, we introduce some notation.

Let $\mathcal{D} = \{(\boldsymbol{x}_i, y_i)\}_{i=1}^n$ be a set of n independent training samples drawn from $\mathcal{Z} = \mathcal{X} \times \mathcal{Y}$ according to a distribution $\mathcal{P}$, where $\mathcal{X}, \mathcal{Y}$ denote the input and label spaces respectively. Let $\mathscr{F} = \{f_\theta : \mathcal{X} \to \mathbb{R}^d \mid \theta \in \Theta\}$ be a class of functions parameterized by $\theta \in \Theta$, mapping input instances to d-dimensional embeddings. Typically, for image tasks, the function is chosen to be a suitable CNN (Krizhevsky et al., 2012). Suppose $X, Y \sim \mathcal{P}$, then define the activation probability $p_j = \mathbb{P}(f_\theta(X)_j \neq 0)$, and its empirical version $\bar{p}_j = \frac{1}{n}\sum_{i=1}^n \mathbb{I}[f_\theta(\boldsymbol{x}_i)_j \neq 0]$.

We now show that sparse embeddings can lead to a quadratic speedup. Consider a d-dimensional sparse query vector $\boldsymbol{u}_q = f_\theta(\boldsymbol{x}_q) \in \mathbb{R}^d$ and a database of n sparse vectors $\{\boldsymbol{v}_i = f_\theta(\boldsymbol{x}^{(i)})\}_{i=1}^n \subset \mathbb{R}^d$ forming a matrix $\boldsymbol{D} \in \mathbb{R}^{n \times d}$. We assume that $\boldsymbol{x}_q, \boldsymbol{x}^{(i)}$ $(i = 1, \ldots, n)$ are sampled independently from $\mathcal{P}$. Computing the vector matrix product $\boldsymbol{D}\boldsymbol{u}_q$ requires looking at only the columns of $\boldsymbol{D}$ corresponding to the non-zero entries of $\boldsymbol{u}_q$ given by $N_q = \{j \mid j \in [1:d], (\boldsymbol{u}_q)_j \neq 0\}$.[1] Furthermore, in each of those columns we only need to look at the non-zero entries. This can be implemented efficiently in practice by storing the non-zero indices for each column in independent lists, as depicted in Figure 1a.

The number of FLOPs incurred is given by,

$$F(\boldsymbol{D}, \boldsymbol{u}_q) = \sum_{j \in N_q} \sum_{i : \boldsymbol{v}_{ij} \neq 0} 1 = \sum_{i=1}^n \sum_{j=1}^d \mathbb{I}[(\boldsymbol{u}_q)_j \neq 0 \wedge \boldsymbol{v}_{ij} \neq 0]$$

[1] We use $[1:d]$ to denote the set $\{1, \ldots, d\}$.

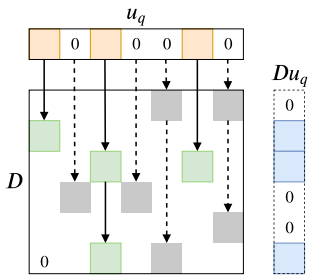

(a) The colored cells denote non-zero entries, and the arrows indicate the list structure for each of the columns, with solid arrows denoting links that were traversed for the given query. The green and grey cells denote the non-zero entries that were accessed and not accessed, respectively. The non-zero values in $\boldsymbol{D}\boldsymbol{u}_q$ (blue) can be computed using only the common non-zero values (green).

(Build Index)
Input: Sparse matrix $\boldsymbol{D}$.
for $j = 1 \cdots d$ **do**
  Init $C[j] \leftarrow \{(i, \boldsymbol{D}_{ij}) \mid \boldsymbol{D}_{ij} \neq 0 \ \wedge \ 1 \leq i \leq n\}$
  (stores the non-zero values and their indices as a list)
end for

(Query)
Input: Sparse query $\boldsymbol{u}_q$.
Init score vector $s[i] = 0, \ 1 \leq i \leq n$.
for $j = 1 \cdots d$ s.t. $\boldsymbol{u}_q[j] \neq 0$ **do**
  for $(i, v) \in C[j]$ **do**
    $s[i] \mathrel{+}= v\boldsymbol{u}_q[j]$
  end for
end for
return s

(b) Efficient algorithm for sparse vector sparse matrix product.

Figure 1

Taking the expectation on both sides w.r.t. $\boldsymbol{x}_q, \boldsymbol{x}^{(i)}$ and using the independence of the data, we get

$$\mathbb{E}[F(\boldsymbol{D}, \boldsymbol{u}_q)] = \sum_{i=1}^{n} \sum_{j=1}^{d} \mathbb{P}\big((\boldsymbol{u}_q)_j \neq 0\big)\mathbb{P}\big(\boldsymbol{v}_{ij} \neq 0\big) = n \sum_{j=1}^{d} \mathbb{P}(f_\theta(X)_j \neq 0)^2 \tag{1}$$

where $X \sim \mathcal{P}$ is an independent random sample. Since the expected number of FLOPs scales linearly with the number of vectors in the database, a more suitable quantity is the *mean-FLOPs-per-row* defined as

$$\mathcal{F}(f_\theta, \mathcal{P}) = \mathbb{E}[F(\boldsymbol{D}, \boldsymbol{u}_q)]/n = \sum_{j=1}^{d} \mathbb{P}(f_\theta(X)_j \neq 0)^2 = \sum_{j=1}^{d} p_j^2. \tag{2}$$

Note that for a fixed amount of sparsity $\sum_{j=1}^{d} p_j = d\,p$, this is minimized when each of the dimensions are non-zero with equal probability $p_j = p, \ \forall j \in [1 : d]$, upon which $\mathcal{F}(f_\theta, \mathcal{P}) = d\,p^2$ (so that as a regularizer, $\mathcal{F}(f_\theta, \mathcal{P})$ will in turn encourage such a uniform distribution across dimensions). Given such a uniform distribution, compared to dense multiplication which has a complexity of $O(d)$ per row, we thus get an improvement by a factor of $1/p^2$ ($p < 1$). Thus when only p fraction of all the entries is non-zero, and evenly distributed across all the columns, we achieve a speedup of $1/p^2$. Note that independence of the non-zero indices is not necessary due to the linearity of expectation.

4 Our Approach

The ℓ_1 regularization is the most common approach to induce sparsity. However, as we will also verify experimentally, it does not ensure an uniform distribution of the non-zeros in all the dimensions that is required for the optimal speed-up. Therefore, we resort to incorporating the actual FLOPs incurred, directly into the loss function which will lead to an optimal trade-off between the search time and accuracy. The FLOPs $\mathcal{F}(f_\theta, \mathcal{P})$ being a discontinuous function of model parameters, is hard to optimize, and hence we will instead optimize using a continuous relaxation of it.

Denote by $\ell(f_\theta, \mathcal{D})$, any metric loss on $\mathcal{D}$ for the embedding function f_θ. The goal in this paper is to minimize the loss while controlling the expected FLOPs $\mathcal{F}(f_\theta, \mathcal{P})$ defined in Eqn. 2. Since the distribution $\mathcal{P}$ is unknown, we use the samples to get an estimate of $\mathcal{F}(f_\theta, \mathcal{P})$. Recall the empirical fraction of non-zero activations $\bar{p}_j = \frac{1}{n}\sum_{i=1}^{n} \mathbb{I}[f_\theta(\boldsymbol{x}_i)_j \neq 0]$, which converges in probability to p_j. Therefore, a consistent estimator for $\mathcal{F}(f_\theta, \mathcal{P})$ based on the samples $\mathcal{D}$ is given by $\mathcal{F}(f_\theta, \mathcal{D}) =$

$\sum_{j=1}^{d} \bar{p}_j^2$. Note that $\mathcal{F}$ denotes either the empirical or population quantities depending on whether the functional argument is $\mathcal{P}$ or $\mathcal{D}$. We now consider the following regularized loss.

$$\min_{\theta \in \Theta} \underbrace{\ell(f_\theta, \mathcal{D}) + \lambda \mathcal{F}(f_\theta, \mathcal{D})}_{\mathcal{L}(\theta)} \tag{3}$$

for some parameter λ that controls the FLOPs-accuracy tradeoff. The regularized loss poses a further hurdle, as $\bar{p}_j$ and consequently $\mathcal{F}(f_\theta, \mathcal{D})$ are not continuous due the presence of the indicator functions. We thus compute the following continuous relaxation. Define the mean absolute activation $a_j = \mathbb{E}[|f_\theta(X)_j|]$ and its empirical version $\bar{a}_j = \frac{1}{n}\sum_{i=1}^{n} |f_\theta(\boldsymbol{x}_i)_j|$, which is the ℓ_1 norm of the activations (scaled by $1/n$) in contrast to the ℓ_0 quasi norm in the FLOPs calculation. Define the relaxations, $\widetilde{\mathcal{F}}(f_\theta, \mathcal{P}) = \sum_{j=1}^{d} a_j^2$ and its consistent estimator $\widetilde{\mathcal{F}}(f_\theta, \mathcal{D}) = \sum_{j=1}^{d} \bar{a}_j^2$. We propose to minimize the following relaxation, which can be optimized using any off-the-shelf stochastic gradient descent optimizer.

$$\min_{\theta \in \Theta} \underbrace{\ell(f_\theta, \mathcal{D}) + \lambda \widetilde{\mathcal{F}}(f_\theta, \mathcal{D})}_{\widetilde{\mathcal{L}}(\theta)}. \tag{4}$$

Sparse Retrieval. During inference, the sparse vector of a query image is first obtained from the learned model and the nearest neighbour is searched in a database of sparse vectors forming a sparse matrix. An efficient algorithm to compute the dot product of the sparse query vector with the sparse matrix is presented in Figure 1b. This consists of first building a list of the non-zero values and their positions in each column. As motivated in Section 3, given a sparse query vector, it is sufficient to only iterate through the non-zero values and the corresponding columns. Using the scores from the above step, a shortlist of candidates having the top scores is first constructed. The shortlisted candidates are further re-ranked using the dense embeddings. The number of candidates is chosen such that the dense re-ranking time does not dominate the sparse ranking time.

Comparison to SDH (Jeong and Song, 2018). It is instructive to contrast our approach with that of SDH (Jeong and Song, 2018). In contrast to the binary hashes in SDH, our approach learns sparse real valued representations. SDH uses a min-cost-max-flow approach in one of the training steps, while we train ours only using SGD. During inference in SDH, a shortlist of candidates is first created by considering the examples in the database that have hashes with non-empty intersections with the query hash. The candidates are further re-ranked using the dense embeddings. The shortlist in our approach on the other hand is constituted of the examples with the top scores from the sparse embeddings.

Comparison to unrelaxed FLOPs regularizer. We provide an experimental comparison of our continuous relaxation based FLOPs regularizer to its unrelaxed variant, showing that the performance of the two are markedly similar. Setting up this experiment requires some analytical simplifications based on recent DNN analyses. We first recall recent results that indicate that the output of a batch norm layer nearly follows a Gaussian distribution (Santurkar et al., 2018), so that in our context, we could make the simplifying approximation that $f_\theta(\boldsymbol{x})_j$ is distributed as $\rho(X)$ where $X \sim \mathcal{N}(\mu_j(\theta), \sigma_j^2(\theta))$, ρ is the ReLU activation, and where we suppress the dependency of μ_j and σ_j on $\mathcal{P}$. We experimentally verify that this assumption holds by minimizing the KS distance (Massey Jr, 1951) between the CDF of $\rho(X)$ with $X \sim \mathcal{N}(\mu, \sigma^2)$ and the empirical CDF of the activations, with respect to μ, σ. Figure 2a shows the empirical CDF and the fitted CDF of $\rho(X)$ for two different architectures. While μ_j, σ_j cannot be tuned independently for $j \in [d]$ due to their dependence on θ, consider a further simplification where the parameters are independent of each other. Suppose for $j \in \{1, 2\}$, $f_\theta(X)_j = \mathrm{ReLU}(X)$ where $X \sim \mathcal{N}(\mu_j, \sigma_j^2)$, and $\theta = (\mu_1, \mu_2, \sigma_1, \sigma_2)$. We analyze how minimizing $\widetilde{\mathcal{F}}(f_\theta, \mathcal{P})$ compares to minimizing $\mathcal{F}(f_\theta, \mathcal{P})$. Note that we consider the population quantities here instead of the empirical quantities, as they are more amenable to theoretical analyses. We also consider the ℓ_1 regularizer as a baseline. We initialize with $\theta = (\mu_1, \mu_2, \sigma_1, \sigma_2) = (-1/4, -1.3, 1, 1)$, and minimize the three quantities w.r.t. θ via gradient descent with infinitesimally small learning rates. For this contrastive analysis, we do not consider the effect of the metric loss. Note that while the empirical quantity $\mathcal{F}(f_\theta, \mathcal{D})$ cannot be optimized via gradient descent, it is possible to do so for its population counterpart $\mathcal{F}(f_\theta, \mathcal{P})$ since it is available in closed form when making Gaussian assumptions. The details of computing the gradients can be found in Appendix A. Figure 2b shows the trajectory of the activation probabilities (p_1, p_2) during optimization. It can be seen that, in contrast to the ℓ_1-regularizer, $\mathcal{F}$ and $\widetilde{\mathcal{F}}$ tend to sparsify the less sparse activation (p_1) at a faster rate, which *corroborates the fact that they encourage an even distribution of non-zeros*.

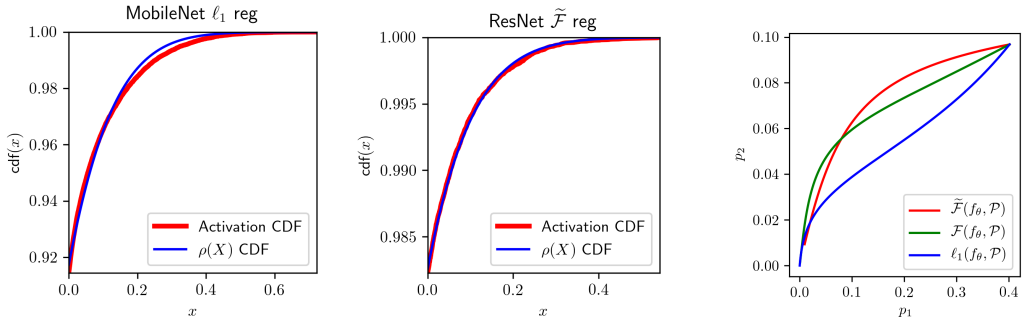

(a) The CDF of $\rho(X)$ fitted to minimize the KS distance to the empirical CDF of the activations for two different architectures.

(b) The trajectory of the activation probabilities when minimizing the respective regularizations.

Figure 2: Figure (a) shows that the CDF of the activations (red) closely resembles the CDF of $\rho(X)$ (blue) where X is a Gaussian random variable. Figure (b) shows that $\mathcal{F}$ and $\widetilde{\mathcal{F}}$ behave similarly by sparsifying the less sparser activation at a faster rate when compared to the ℓ_1 regularizer.

$\widetilde{\mathcal{F}}$ promotes orthogonality. We next show that when the embeddings are normalized to have a unit norm, as typically done in metric learning, then minimizing $\widetilde{\mathcal{F}}(f_\theta, \mathcal{D})$ is equivalent to promoting orthogonality on the absolute values of the embedding vectors. Let $\|f_\theta(\boldsymbol{x})\|_2 = 1,\ \forall x \in \mathcal{X}$, we then have the following:

$$\widetilde{\mathcal{F}}(f_\theta, \mathcal{D}) = \sum_{j=1}^{d} \left(\frac{1}{n} \sum_{i=1}^{n} |f_\theta(\boldsymbol{x}_i)_j| \right)^2 = \frac{1}{n^2} \sum_{p,q \in [1:n]} \left\langle |f_\theta(\boldsymbol{x}_p)|, |f_\theta(\boldsymbol{x}_q)| \right\rangle \tag{5}$$

$\widetilde{\mathcal{F}}(f_\theta, \mathcal{D})$ is minimized when the vectors $\{|f_\theta(\boldsymbol{x}_i)|\}_{i=1}^n$ are orthogonal. Metric learning losses aim at minimizing the interclass dot product, whereas the FLOPs regularizer aims at minimizing pairwise dot products irrespective of the class, leading to a tradeoff between sparsity and accuracy. This approach of pushing the embeddings apart, bears some resemblance to the idea of *spreading vectors* (Sablayrolles et al., 2019) where an entropy based regularizer is used to uniformly distribute the embeddings on the unit sphere, albeit without considering any sparsity. Maximizing the pairwise dot product helps in reducing FLOPs as is illustrated by the following toy example. Consider a set of d vectors $\{\boldsymbol{v}_i\}_{i=1}^d \subset \mathbb{R}^d$ (here $n = d$) satisfying $\|\boldsymbol{v}_i\|_2 = 1,\ \forall i \in [1:d]$. Then $\sum_{p,q \in [1:d]} \left\langle |\boldsymbol{v}_p|, |\boldsymbol{v}_q| \right\rangle$ is minimized when $\boldsymbol{v}_p = e_p$, where e_p is an one-hot vector with the p th entry equal to 1 and the rest 0. The FLOPs regularizer thus tends to spread out the non-zero activations in all the dimensions, thus producing balanced embeddings. This simple example also demonstrates that when the number of classes in the training set is smaller or equal to the number of dimensions d, a trivial embedding that minimizes the metric loss and also achieves a small number of FLOPs is $f_\theta(\boldsymbol{x}) = e_y$ where y is true label for $\boldsymbol{x}$. This is equivalent to predicting the class of the input instance. The caveat with such embeddings is that they might not be semantically meaningful beyond the specific supervised task, and will naturally hurt performance on unseen classes, and tasks where the representation itself is of interest. In order to avoid such a collapse in our experiments, we ensure that the embedding dimension is smaller than the number of training classes. Furthermore, as recommended by Sablayrolles et al. (2017), we perform all our evaluations on unseen classes.

5 Experiments

We evaluate our proposed approach on a large scale metric learning dataset: the Megaface (Kemelmacher-Shlizerman et al., 2016) used for face recognition. This is a much more fine grained retrieval tasks (with 85k classes for training) compared to the datasets used by Jeong and Song (2018). This dataset also satisfies our requirement of the number of classes being orders of magnitude higher than the dimensions of the sparse embedding. As discussed in Section 4, a few number of classes during training can lead the model to simply learn an encoding of the training classes and thus not generalize to unseen classes. Face recognition datasets avoid this situation by virtue of the huge number of training classes and a balanced distribution of examples across all the classes.

Following standard protocol for evaluation on the Megaface dataset (Kemelmacher-Shlizerman et al., 2016), we train on a refined version of the MSCeleb-1M (Guo et al., 2016) dataset released by Deng et al. (2018) consisting of 1 million images spanning 85k classes. We evaluate with 1 million distractors from the Megaface dataset and 3.5k query images from the Facescrub dataset (Ng and Winkler, 2014), which were not seen during training.

Network Architecture. We experiment with two architectures: MobileFaceNet (Chen et al., 2018), and ResNet-101 (He et al., 2016). We use ReLU activations in the embedding layer for MobileFaceNet, and SThresh activations for ResNet. The activations are ℓ_2-normalized to produce an embedding on the unit sphere, and used to compute the Arcface loss (Deng et al., 2018). We learn 1024 dimensional sparse embeddings for the ℓ_1 and $\widetilde{\mathcal{F}}$ regularizers; and 128, 512 dimensional dense embeddings as baselines. All models were implemented in Tensorflow (Abadi et al., 2016) with the sparse retrieval algorithm implemented in C++.[2] The re-ranking step used 512-d dense embeddings.

Activation Function. In practice, having a non-linear activation at the embedding layer is crucial for sparsification. Layers with activations such as ReLU are easier to sparsify due to the bias parameter in the layer before the activation (linear or batch norm) which acts as a direct control knob to the sparsity. More specifically, $\mathrm{ReLU}(\boldsymbol{x} - \boldsymbol{\lambda})$ can be made more (less) sparse by increasing (decreasing) the components of $\boldsymbol{\lambda}$, where $\boldsymbol{\lambda}$ is the bias parameter of the previous linear layer. In this paper we consider two types of activations: $\mathrm{ReLU}(\boldsymbol{x}) = \max(\boldsymbol{x}, \boldsymbol{0})$, and the soft thresholding operator $\mathrm{SThresh}(\boldsymbol{x}) = \mathrm{sgn}(\boldsymbol{x}) \max(|\boldsymbol{x}| - 1/2, 0)$ (Boyd and Vandenberghe, 2004). ReLU activations always produce positive values, whereas soft thresholding can produce negative values as well. The analysis in Figure 2 follows similarly for SThresh using the fact that $|\mathrm{SThresh}(X)| = \mathrm{ReLU}(X - 1/2) + \mathrm{ReLU}(-X - 1/2)$.

Practical Considerations. In practice, setting a large regularization weight λ from the beginning is harmful for training. Sparsifying too quickly using a large λ leads to many dead activations (saturated to zero) in the embedding layer and the model getting stuck in a local minima. Therefore, we use an annealing procedure and gradually increase λ throughout the training using a regularization weight schedule $\lambda(t) : \mathbb{N} \mapsto \mathbb{R}$ that maps the training step to a real valued regularization weight. In our experiments we choose a $\lambda(t)$ that increases quadratically as $\lambda(t) = \lambda(t/T)^2$, until step $t = T$, where T is the threshold step beyond which $\lambda(t) = \lambda$.

Baselines. We compare our proposed $\widetilde{\mathcal{F}}$-regularizer, with multiple baselines: exhaustive search with dense embeddings, sparse embeddings using ℓ_1 regularization, *Sparse Deep Hashing (SDH)* (Jeong and Song, 2018), and PCA, LSH, PQ applied to the 512 dimensional dense embeddings from both the architectures. We train the SDH model using the aforementioned architectures for 512 dimensional embeddings, with number of active hash bits $k = 3$. We use numpy (using efficient MKL optimizations in the backend) for matrix multiplication required for exhaustive search in the dense and PCA baselines. We use the CPU version of the *Faiss* (Johnson et al., 2017) library for LSH and PQ (we use the IVF-PQ index from Faiss).

Further details on the training hyperparameters and the hardware used can be found in Appendix B.

5.1 Results

We report the recall and the time-per-query for various hyperparameters of our proposed approach and the baselines, yielding trade-off curves. The reported times include the time required for re-ranking. The trade-off curves for MobileNet and ResNet are shown in Figures 3a and 3c respectively. We observe that while vanilla ℓ_1 regularization is an improvement by itself for some hyperparameter settings, the $\widetilde{\mathcal{F}}$ regularizer is a further improvement, and yields the most optimal trade-off curve. SDH has a very poor speed-accuracy trade-off, which is mainly due to the explosion in the number of shortlisted candidates with increasing number of active bits leading to an increase in the retrieval time. On the other hand, while having a small number of active bits is faster, it leads to a smaller recall. For the other baselines we notice the usual order of performance, with PQ having the best speed-up compared to LSH and PCA. While dimensionality reduction using PCA leads to some speed-up for relatively high dimensions, it quickly wanes off as the dimension is reduced even further.

We also report the sub-optimality ratio $R_{sub} = \mathcal{F}(f_\theta, \mathcal{D})/d\bar{p}^2$ computed over the dataset $\mathcal{D}$, where $\bar{p} = \frac{1}{d}\sum_{j=1}^{d} \bar{p}_j$ is the mean activation probability estimated on the test data. Notice that $R \geq 1$, and

[2]The implementation code and trained models will be made publicly available after acceptance.

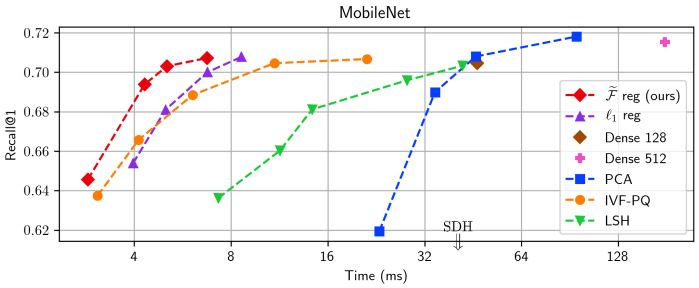

(a) Time per query vs recall for MobileNet.

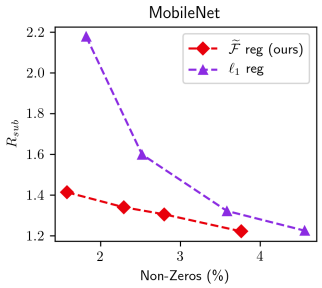

(b) R_{sub} vs sparsity for MobileNet.

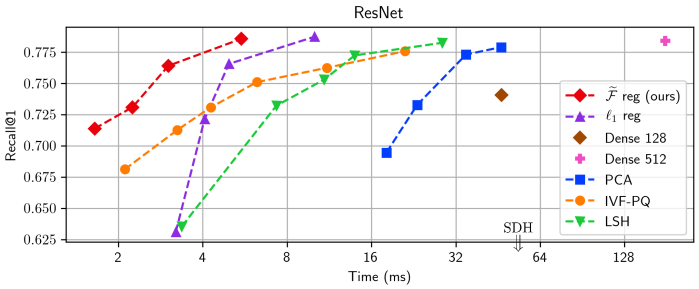

(c) Time per query vs recall for ResNet.

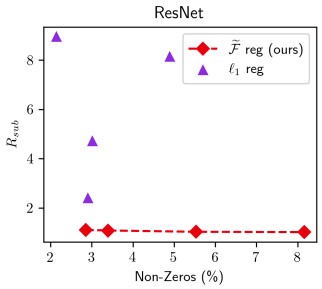

(d) R_{sub} vs sparsity for ResNet.

Figure 3: Figures (a) and (c) show the speed vs recall trade-off for the MobileNet and ResNet architectures respectively. The trade-off curves produced by varying the hyper-parameters of the respective approaches. The points with higher recall and lower time (top-left side of the plots) are better. The SDH baseline being out of range of both the plots is indicated using an arrow. Figures (b) and (d) show the sub-optimality ratio vs sparsity plots for MobileNet and ResNet respectively. R_{sub} closer to 1 indicates that the non-zeros are uniformly distributed across the dimensions.

the optimal $R = 1$ is achieved when $\bar{p}_j = \bar{p},\ \forall j \in [1 : d]$, that is when the non-zeros are evenly distributed across the dimensions. The sparsity-vs-suboptimality plots for MobileNet and ResNet are shown in Figures 3a and 3c respectively. We notice that the $\widetilde{\mathcal{F}}$-regularizer yields values of R closer to 1 when compared to the ℓ_1-regularizer. For the MobileNet architecture we notice that the ℓ_1 regularizer is able to achieve values of R close to that of $\widetilde{\mathcal{F}}$ in the less sparser region. However, the gap increases substantially with increasing sparsity. For the ResNet architecture on the other hand the ℓ_1 regularizer yields extremely sub-optimal embeddings in all regimes. The $\widetilde{\mathcal{F}}$ regularizer is therefore able to produce more balanced distribution of non-zeros.

The sub-optimality is also reflected in the recall values. The gap in the recall values of the ℓ_1 and $\widetilde{\mathcal{F}}$ models is much higher when the sub-optimality gap is higher, as in the case of ResNet, while it is small when the sub-optimality gap is smaller as in the case of MobileNet. This shows the significance of having a balanced distribution of non-zeros.

6 Conclusion

In this paper we proposed a novel approach to learn high dimensional embeddings with the goal of improving efficiency of retrieval tasks. Our approach integrates the FLOPs incurred during retrieval into the loss function as a regularizer and optimizes it directly through a continuous relaxation. We provide further insight into our approach by showing that the proposed approach favors an even distribution of the non-zero activations across all the dimensions. We experimentally showed that our approach indeed leads to a more even distribution when compared to the ℓ_1 regularizer. We compared our approach to a number of other baselines and showed that it has a better speed-vs-accuracy trade-off. Overall we were able to show that sparse embeddings can be around 50$\times$ faster compared to dense embeddings without a significant loss of accuracy.

REFERENCES

Martín Abadi, Paul Barham, Jianmin Chen, Zhifeng Chen, Andy Davis, Jeffrey Dean, Matthieu Devin, Sanjay Ghemawat, Geoffrey Irving, Michael Isard, et al. Tensorflow: A system for large-scale machine learning. In *12th USENIX Symposium on Operating Systems Design and Implementation (OSDI 16)*, pages 265–283, 2016.

Alexandr Andoni, Piotr Indyk, Thijs Laarhoven, Ilya Razenshteyn, and Ludwig Schmidt. Practical and optimal lsh for angular distance. *NeurIPS*, 2015.

Alex Auvolat, Sarath Chandar, Pascal Vincent, Hugo Larochelle, and Yoshua Bengio. Clustering is efficient for approximate maximum inner product search. *arXiv preprint arXiv:1507.05910*, 2015.

Dmitry Baranchuk, Artem Babenko, and Yury Malkov. Revisiting the inverted indices for billion-scale approximate nearest neighbors. In *Proceedings of the European Conference on Computer Vision (ECCV)*, pages 202–216, 2018.

Stephen Boyd and Lieven Vandenberghe. *Convex optimization*. Cambridge university press, 2004.

Yue Cao, Mingsheng Long, Jianmin Wang, Han Zhu, and Qingfu Wen. Deep quantization network for efficient image retrieval. *AAAI*, 2016.

Yue Cao, Mingsheng Long, Bin Liu, and Jianmin Wang. Deep cauchy hashing for hamming space retrieval. In *Proceedings of the IEEE Conference on Computer Vision and Pattern Recognition*, pages 1229–1237, 2018.

Moses S Charikar. Similarity estimation techniques from rounding algorithms. In *Proceedings of the thiry-fourth annual ACM symposium on Theory of computing*, pages 380–388. ACM, 2002.

Sheng Chen, Yang Liu, Xiang Gao, and Zhen Han. Mobilefacenets: Efficient cnns for accurate real-time face verification on mobile devices. *arXiv preprint arXiv:1804.07573*, 2018.

Sanjoy Dasgupta, Charles F Stevens, and Saket Navlakha. A neural algorithm for a fundamental computing problem. *Science*, 2017.

Jiankang Deng, Jia Guo, and Stefanos Zafeiriou. Arcface: Additive angular margin loss for deep face recognition. *arXiv preprint arXiv:1801.07698*, 2018.

Venice Erin Liong, Jiwen Lu, Gang Wang, Pierre Moulin, and Jie Zhou. Deep hashing for compact binary codes learning. *CVPR*, 2015.

Tiezheng Ge, Kaiming He, Qifa Ke, and Jian Sun. Optimized product quantization for approximate nearest neighbor search. *CVPR*, 2013.

Aristides Gionis, Piotr Indyk, Rajeev Motwani, et al. Similarity search in high dimensions via hashing. *VLDB*, 1999.

Yandong Guo, Lei Zhang, Yuxiao Hu, Xiaodong He, and Jianfeng Gao. MS-Celeb-1M: A dataset and benchmark for large scale face recognition. In *European Conference on Computer Vision*. Springer, 2016.

M Hadi Kiapour, Xufeng Han, Svetlana Lazebnik, Alexander C Berg, and Tamara L Berg. Where to buy it: Matching street clothing photos in online shops. In *Proceedings of the IEEE international conference on computer vision*, pages 3343–3351, 2015.

Kaiming He, Xiangyu Zhang, Shaoqing Ren, and Jian Sun. Identity mappings in deep residual networks. In *European conference on computer vision*, pages 630–645. Springer, 2016.

Geoffrey E Hinton and Ruslan R Salakhutdinov. Reducing the dimensionality of data with neural networks. *science*, 313(5786):504–507, 2006.

Herve Jegou, Matthijs Douze, and Cordelia Schmid. Product quantization for nearest neighbor search. *TPAMI*, 2011.

Yeonwoo Jeong and Hyun Oh Song. Efficient end-to-end learning for quantizable representations. *ICML*, 2018.

Yushi Jing, David Liu, Dmitry Kislyuk, Andrew Zhai, Jiajing Xu, Jeff Donahue, and Sarah Tavel. Visual search at pinterest. In *Proceedings of the 21th ACM SIGKDD International Conference on Knowledge Discovery and Data Mining*, pages 1889–1898. ACM, 2015.

Jeff Johnson, Matthijs Douze, and Hervé Jégou. Billion-scale similarity search with gpus. *arXiv preprint arXiv:1702.08734*, 2017.

Ira Kemelmacher-Shlizerman, Steven M Seitz, Daniel Miller, and Evan Brossard. The megaface benchmark: 1 million faces for recognition at scale. *CVPR*, 2016.

Douwe Kiela and Léon Bottou. Learning image embeddings using convolutional neural networks for improved multi-modal semantics. In *Proceedings of the 2014 Conference on Empirical Methods in Natural Language Processing (EMNLP)*, pages 36–45, 2014.

Diederik P Kingma and Max Welling. Auto-encoding variational bayes. *arXiv preprint arXiv:1312.6114*, 2013.

Gregory Koch, Richard Zemel, and Ruslan Salakhutdinov. Siamese neural networks for one-shot image recognition. In *ICML Deep Learning Workshop*, volume 2, 2015.

Deguang Kong, Ryohei Fujimaki, Ji Liu, Feiping Nie, and Chris Ding. Exclusive feature learning on arbitrary structures via $ell_{1,2}$-norm. In *Advances in Neural Information Processing Systems*, pages 1655–1663, 2014.

Alex Krizhevsky, Ilya Sutskever, and Geoffrey E Hinton. Imagenet classification with deep convolutional neural networks. *NeurIPS*, 2012.

Qi Li, Zhenan Sun, Ran He, and Tieniu Tan. Deep supervised discrete hashing. *NeurIPS*, 2017.

Wenye Li, Jingwei Mao, Yin Zhang, and Shuguang Cui. Fast similarity search via optimal sparse lifting. *NeurIPS*, 2018.

Baoyuan Liu, Min Wang, Hassan Foroosh, Marshall Tappen, and Marianna Pensky. Sparse convolutional neural networks. In *Proceedings of the IEEE Conference on Computer Vision and Pattern Recognition*, pages 806–814, 2015.

Weiyang Liu, Yandong Wen, Zhiding Yu, and Meng Yang. Large-margin softmax loss for convolutional neural networks. In *ICML*, volume 2, page 7, 2016.

David G Lowe. Distinctive image features from scale-invariant keypoints. *International journal of computer vision*, 2004.

Laurens van der Maaten and Geoffrey Hinton. Visualizing data using t-sne. *Journal of machine learning research*, 9(Nov):2579–2605, 2008.

Yury Malkov, Alexander Ponomarenko, Andrey Logvinov, and Vladimir Krylov. Approximate nearest neighbor algorithm based on navigable small world graphs. *Information Systems*, 2014.

Yury A Malkov and Dmitry A Yashunin. Efficient and robust approximate nearest neighbor search using hierarchical navigable small world graphs. *TPAMI*, 2018.

Frank J Massey Jr. The kolmogorov-smirnov test for goodness of fit. *Journal of the American statistical Association*, 46(253):68–78, 1951.

Lukas Meier, Sara Van De Geer, and Peter Bühlmann. The group lasso for logistic regression. *Journal of the Royal Statistical Society: Series B (Statistical Methodology)*, 70(1):53–71, 2008.

Yair Movshovitz-Attias, Alexander Toshev, Thomas K Leung, Sergey Ioffe, and Saurabh Singh. No fuss distance metric learning using proxies. *arXiv preprint arXiv:1703.07464*, 2017.

Paul Neculoiu, Maarten Versteegh, and Mihai Rotaru. Learning text similarity with siamese recurrent networks. In *Proceedings of the 1st Workshop on Representation Learning for NLP*, pages 148–157, 2016.

Behnam Neyshabur and Nathan Srebro. On symmetric and asymmetric lshs for inner product search. In *International Conference on Machine Learning*, pages 1926–1934, 2015.

Hong-Wei Ng and Stefan Winkler. A data-driven approach to cleaning large face datasets. In *Image Processing (ICIP), 2014 IEEE International Conference on*. IEEE, 2014.

Qingqun Ning, Jianke Zhu, Zhiyuan Zhong, Steven CH Hoi, and Chun Chen. Scalable image retrieval by sparse product quantization. *IEEE Transactions on Multimedia*, 19(3):586–597, 2016.

Mohammad Norouzi, David J Fleet, and Ruslan R Salakhutdinov. Hamming distance metric learning. *NeurIPS*, 2012.

Hyun Oh Song, Stefanie Jegelka, Vivek Rathod, and Kevin Murphy. Deep metric learning via facility location. In *Proceedings of the IEEE Conference on Computer Vision and Pattern Recognition*, pages 5382–5390, 2017.

Maxim Raginsky and Svetlana Lazebnik. Locality-sensitive binary codes from shift-invariant kernels. *NeurIPS*, 2009.

Parikshit Ram and Alexander G Gray. Maximum inner-product search using cone trees. In *Proceedings of the 18th ACM SIGKDD international conference on Knowledge discovery and data mining*, pages 931–939. ACM, 2012.

Alexandre Sablayrolles, Matthijs Douze, Nicolas Usunier, and Hervé Jégou. How should we evaluate supervised hashing? In *2017 IEEE International Conference on Acoustics, Speech and Signal Processing (ICASSP)*, pages 1732–1736. IEEE, 2017.

Alexandre Sablayrolles, Matthijs Douze, Cordelia Schmid, and Hervé Jégou. Spreading vectors for similarity search. *ICLR*, 2019.

Shibani Santurkar, Dimitris Tsipras, Andrew Ilyas, and Aleksander Madry. How does batch normalization help optimization? In *Advances in Neural Information Processing Systems*, pages 2483–2493, 2018.

Florian Schroff, Dmitry Kalenichenko, and James Philbin. Facenet: A unified embedding for face recognition and clustering. In *Proceedings of the IEEE conference on computer vision and pattern recognition*, pages 815–823, 2015.

Devashish Shankar, Sujay Narumanchi, HA Ananya, Pramod Kompalli, and Krishnendu Chaudhury. Deep learning based large scale visual recommendation and search for e-commerce. *arXiv preprint arXiv:1703.02344*, 2017.

Anshumali Shrivastava and Ping Li. Asymmetric lsh (alsh) for sublinear time maximum inner product search (mips). In *Advances in Neural Information Processing Systems*, pages 2321–2329, 2014.

Robert Tibshirani. Regression shrinkage and selection via the lasso. *Journal of the Royal Statistical Society: Series B (Methodological)*, 58(1):267–288, 1996.

Jingdong Wang, Ting Zhang, Nicu Sebe, Heng Tao Shen, et al. A survey on learning to hash. *IEEE transactions on pattern analysis and machine intelligence*, 40(4):769–790, 2018.

Xueyi Wang. A fast exact k-nearest neighbors algorithm for high dimensional search using k-means clustering and triangle inequality. In *Neural Networks (IJCNN), The 2011 International Joint Conference on*, pages 1293–1299. IEEE, 2011.

Kilian Q Weinberger and Lawrence K Saul. Distance metric learning for large margin nearest neighbor classification. *Journal of Machine Learning Research*, 10(Feb):207–244, 2009.

Yair Weiss, Antonio Torralba, and Rob Fergus. Spectral hashing. *NeurIPS*, 2009.

Wei Wen, Chunpeng Wu, Yandan Wang, Yiran Chen, and Hai Li. Learning structured sparsity in deep neural networks. In *Advances in neural information processing systems*, pages 2074–2082, 2016.

Yang Zhou, Rong Jin, and Steven Chu-Hong Hoi. Exclusive lasso for multi-task feature selection. In *Proceedings of the Thirteenth International Conference on Artificial Intelligence and Statistics*, pages 988–995, 2010.

Appendix

A GRADIENT COMPUTATIONS

Consider a random variable $X \sim \mathcal{N}(\mu, \sigma^2)$ with $\mu \leq 0$. Define $X_+ = \max(X, 0)$. The we can prove the following Lemmas.

Lemma 1.

$$\mathbb{E}[X_+] = \frac{\sigma}{\sqrt{2\pi}} \exp\left(-\frac{\mu^2}{2\sigma^2}\right) + \mu\left(1 - \Phi\left(-\frac{\mu}{\sigma}\right)\right), \tag{6}$$

and,

$$\mathbb{P}(X \neq 0) = 1 - \Phi\left(-\frac{\mu}{\sigma}\right) \tag{7}$$

Proof. The proof is based on standard Gaussian identities.

$$\begin{aligned}
\mathbb{E}[X_+] &= \int_0^\infty \frac{x}{\sqrt{2\pi\sigma^2}} \exp\left(-\frac{(x-\mu)^2}{2\sigma^2}\right) dx = \int_{-\mu}^\infty \frac{x+\mu}{\sqrt{2\pi\sigma^2}} \exp\left(-\frac{x^2}{2\sigma^2}\right) dx \\
&= \int_{-\mu}^\infty \frac{x}{\sqrt{2\pi\sigma^2}} \exp\left(-\frac{x^2}{2\sigma^2}\right) dx + \int_{-\mu}^\infty \frac{\mu}{\sqrt{2\pi\sigma^2}} \exp\left(-\frac{x^2}{2\sigma^2}\right) dx \\
&= \frac{\sigma}{\sqrt{2\pi}} \exp\left(-\frac{\mu^2}{2\sigma^2}\right) + \mu\left(1 - \Phi\left(-\frac{\mu}{\sigma}\right)\right)
\end{aligned}$$

$$\begin{aligned}
\mathbb{P}(X \neq 0) &= \int_0^\infty \frac{1}{\sqrt{2\pi\sigma^2}} \exp\left(-\frac{(x-\mu)^2}{2\sigma^2}\right) dx = \int_{-\mu/\sigma}^\infty \frac{1}{\sqrt{2\pi}} \exp\left(-\frac{x^2}{2}\right) dx \\
&= 1 - \Phi\left(-\frac{\mu}{\sigma}\right)
\end{aligned}$$

□

Lemma 2.

$$\frac{\partial}{\partial\mu}\mathbb{P}(X \neq 0) = -\frac{\partial}{\partial\mu}\Phi\left(-\frac{\mu}{\sigma}\right) = \frac{1}{\sigma\sqrt{2\pi}} \exp\left(-\frac{\mu^2}{2\sigma^2}\right) \tag{8}$$

$$\frac{\partial}{\partial\sigma}\mathbb{P}(X \neq 0) = -\frac{\partial}{\partial\sigma}\Phi\left(-\frac{\mu}{\sigma}\right) = -\frac{\mu}{\sigma^2\sqrt{2\pi}} \exp\left(-\frac{\mu^2}{2\sigma^2}\right) \tag{9}$$

Proof. Follows directly from the statement by standard differentiation. □

Lemma 3.

$$\frac{\partial}{\partial\mu}\mathbb{E}[X_+] = 1 - \Phi\left(-\frac{\mu}{\sigma}\right) \tag{10}$$

$$\frac{\partial}{\partial\sigma}\mathbb{E}[X_+] = \frac{1}{\sqrt{2\pi}} \exp\left(-\frac{\mu^2}{2\sigma^2}\right) \tag{11}$$

Proof.

$$\frac{\partial}{\partial\mu}\mathbb{E}[X_+] = -\frac{\mu}{\sigma\sqrt{2\pi}} \exp\left(-\frac{\mu^2}{2\sigma^2}\right) + \frac{\partial}{\partial\mu}\left[\mu\left(1 - \Phi\left(-\frac{\mu}{\sigma}\right)\right)\right] = 1 - \Phi\left(-\frac{\mu}{\sigma}\right)$$

where the last step follows from Lemma 2.

$$\begin{aligned}
\frac{\partial}{\partial\sigma}\mathbb{E}[X_+] &= \frac{1}{\sqrt{2\pi}} \exp\left(-\frac{\mu^2}{2\sigma^2}\right) + \frac{\mu^2}{\sigma^2\sqrt{2\pi}} \exp\left(-\frac{\mu^2}{2\sigma^2}\right) + \frac{\partial}{\partial\sigma}\left[\mu\left(1 - \Phi\left(-\frac{\mu}{\sigma}\right)\right)\right] \\
&= \frac{1}{\sqrt{2\pi}} \exp\left(-\frac{\mu^2}{2\sigma^2}\right)
\end{aligned}$$

where the last step follows from Lemma 2. □

Lemma 4.

$$\frac{\partial}{\partial \mu}\mathbb{E}[X_+]^2 = 2\mathbb{E}[X_+]\left(1-\Phi\left(-\frac{\mu}{\sigma}\right)\right) \tag{12}$$

$$\frac{\partial}{\partial \sigma}\mathbb{E}[X_+]^2 = 2\mathbb{E}[X_+]\frac{1}{\sqrt{2\pi}}\exp\left(-\frac{\mu^2}{2\sigma^2}\right) \tag{13}$$

Proof. Follows directly from Lemma 3. □

Lemma 5.

$$\frac{\partial}{\partial \mu}\mathbb{P}(X\neq 0)^2 = 2\mathbb{P}(X\neq 0)\frac{1}{\sigma\sqrt{2\pi}}\exp\left(-\frac{\mu^2}{2\sigma^2}\right) \tag{14}$$

$$\frac{\partial}{\partial \sigma}\mathbb{P}(X\neq 0)^2 = -2\mathbb{P}(X\neq 0)\frac{\mu}{\sigma^2\sqrt{2\pi}}\exp\left(-\frac{\mu^2}{2\sigma^2}\right) \tag{15}$$

Proof. Follows directly from Lemma 2. □

B EXPERIMENTAL DETAILS

All images were resized to size 112×112 and aligned using a pre-trained aligner[3]. For the Arcloss function, we used the recommended parameters of margin $m = 0.5$ and temperature $s = 64$. We trained our models on 4 NVIDIA Tesla V-100 GPUs using SGD with a learning rate of 0.001, momentum of 0.9. Both the architectures were trained for a total of 230k steps, with the learning rate being decayed by a factor of 10 after 170k steps. We use a batch size of 256 and 64 per GPU for MobileFaceNet for ResNet respectively.

Pre-training in SDH is performed in the same way as described above. The hash learning step is trained on a single GPU with a learning rate of 0.001. The ResNet model is trained for 200k steps with a batch size of 64, and the MobileFaceNet model is trained for 150k steps with a batch size of 256. We set the number of active bits $k = 3$ and a pairwise cost of $p = 0.1$.

Hyper-parameters for MobileNet models.

1. The regularization parameter λ for the $\widetilde{\mathcal{F}}$ regularizer was varied as 200, 300, 400, 600.
2. The regularization parameter λ for the ℓ_1 regularizer was varied as 1.5, 2.0, 2.7, 3.5.
3. The PCA dimension is varied as 64, 96, 128, 256.
4. The number of LSH bits were varied as 512, 768, 1024, 2048, 3072.
5. For IVF-PQ from the faiss library, the following parameters were fixed: `nlist=4096, M=64, nbit=8`, and `nprobe` was varied as 100, 150, 250, 500, 1000.

Hyper-parameters for ResNet baselines.

1. The regularization parameter λ for the $\widetilde{\mathcal{F}}$ regularizer was varied as 50, 100, 200, 630.
2. The regularization parameter λ for the ℓ_1 regularizer was varied as 2.0, 3.0, 5.0, 6.0.
3. The PCA dimension is varied as 48, 64, 96, 128.
4. The number of LSH bits were varied as 256, 512, 768, 1024, 2048.
5. For IVF-PQ, the following parameters were the same as in MobileNet: `nlist=4096, M=64, nbit=8`. `nprobe` was varied as 50, 100, 150, 250, 500, 1000.

[3] `https://github.com/deepinsight/insightface`

Re-ranking. We use the following heuristic to create the shortlist of candidates after the sparse ranking step. We first shortlist all candidates with a score greater than some confidence threshold. For our experiments we set the confidence threshold to be equal to 0.25. If the size of this shortlist is larger than k, it is further shrunk by consider the top k scorers. For all our experiments we set $k = 1000$. This heuristic avoids sorting the whole array, which can be a bottleneck in this case. The parameters are chosen such that the time required for the re-ranking step does not dominate the total retrieval time.

Hardware.

1. All models were trained on 4 NVIDIA Tesla V-100 GPUs with 16G of memory.
2. System Memory: 256G.
3. CPU: Intel(R) Xeon(R) CPU E5-2686 v4 @ 2.30GHz.
4. Number of threads: 32.
5. Cache: L1d cache 32K, L1i cache 32K, L2 cache 256K, L3 cache 46080K.

All timing experiments were performed on a single thread in isolation.